Letter

Reductant-Activated, High-Coverage, Covalent Functionalization of 1T#-MoS

Ellen X. Yan, Miguel Cabán-Acevedo, Kimberly M. Papadantonakis, Bruce S. Brunschwig, and Nathan S. Lewis

ACS Materials Lett., **Just Accepted Manuscript** • DOI: 10.1021/acsmaterialslett.9b00241 • Publication Date (Web): 20 Dec 2019

Reductant-Activated, High-Coverage, Covalent Functionalization of 1T′-MoS_2

Ellen X. Yan,[†] Miguel Cabán-Acevedo,[†] Kimberly M. Papadantonakis,[†] Bruce S. Brunschwig,[‡] and Nathan S. Lewis*[,†,‡]

[†]Division of Chemistry and Chemical Engineering, [‡]Beckman Institute, California Institute of Technology, Pasadena, California 91125, United States

ABSTRACT: Recently developed covalent functionalization chemistry for MoS_2 in the 1T′ phase enables the formation of covalent chalcogenide-carbon bonds from alkyl halides and aryl diazonium salts. However, the coverage of functional groups using this method has been limited by the negative charge stored in the exfoliated MoS_2 sheets to <25-30% per MoS_2 unit. We report herein a reductant-activated functionalization wherein one-electron metallocene reductants, such as nickelocene, octamethylnickelocene, and cobaltocene, are introduced during functionalization with methyl and propyl halides to tune the coverage of the alkyl groups. The reductant-activated functionalization yields functional group coverages up to 70%, ~ 1.5–2 times higher than the previous limit, and enables functionalization by weak electrophiles, such as 1-chloropropane, that are otherwise unreactive with chemically exfoliated MoS_2. We also explored the dependence of coverage on the strength of the leaving group and the steric hindrance of the alkyl halide in the absence of reductants, and showed that functionalization was ineffective for chloride leaving groups and for secondary and tertiary alkyl iodides. These results demonstrate a substantial increase in coverage compared to functionalization without reductants, and may impact the performance of these materials in applications reliant on surface interactions. Furthermore, this method may be applicable to the covalent functionalization of similar layered materials and metal chalcogenides.

Crystalline molybdenum disulfide (MoS_2) consists of layers of two-dimensional sheets held together by van der Waals forces. Monolayers and few-layer-films of MoS_2 can be produced by chemical and mechanical exfoliation of bulk crystals or by chemical-vapor deposition (CVD).[1-2] These materials have been explored for applications in photovoltaics,[3-4] transistors,[5] ultra-thin flexible electronics,[6] sensors,[7-9] nanofiltration,[10] drug delivery,[11] and biological imaging.[12] Macroscale areas of such monolayers have been used in photovoltaic and photoelectrochemical devices, whereas exfoliated sheets with nanoscale areas have been used in catalysis, drug delivery, and biological imaging.[13-16]

MoS_2 has several common polymorphs, including the semiconducting 2H and 3R phases as well as the metallic 1T phase (Figure S1). In the phase nomenclature, the initial integer represents the number of layers in the unit cell, and the letter represents the type of symmetry (H = hexagonal, R = rhombohedral, T = tetragonal). The 2H phase is the thermodynamically stable form.[17-20] Multilayer MoS_2 can be chemically exfoliated by lithium intercalation (*ce*MoS_2) which induces a phase transformation from 2H to 1T.[21] Studies of restacked *ce*MoS_2, by transmission-electron microscopy (TEM) and scanning-tunneling microscopy (STM), have shown that a distorted 1T-type phase, 1T', with a 2 × 1 supercell lattice containing zig-zag chains is predominant over the pristine octahedral 1T phase.[21-22] Intercalation for extended time periods yields complete conversion to the distorted 1T′ phase (Figure S1).[23] Theoretical calculations in support of these experimental observations demonstrate that the 1T′ phase is more stable than the 1T phase and predict that the 1T′ phase has a band gap of 0.1-0.2 eV, in contrast to the metallic 1T phase.[23-25] Some reports refer to the predominant phase in *ce*MoS_2 as 1T-MoS_2, while acknowledging that this 1T phase may actually be the distorted 1T′ phase.[26] Considering the currently available density-functional-theory (DFT) calculations and experimental data, which collectively suggest the 1T′ is predominant over the 1T phase in *ce*MoS_2, we refer to the predominant 1T-type phase as 1T′ in this manuscript.[21-25] Conversion of the metastable 1T′ phase to the thermodynamically stable 2H phase requires overcoming a small activation barrier, either by annealing at 300 °C or by laser treatment.[26-27]

Organic functionalization of semiconductor surfaces can be used to passivate sites of corrosion or charge-carrier recombination,[28] introduce surface dipoles to tune the relative energy of the band-edges,[29-30] or provide chemical functionality for subsequent reactions.[31] These applications are sensitive to the degree of surface coverage of the functional groups. 2H-MoS_2 has a relatively inert basal plane that limits the chemical functionalization that can be achieved. However, several routes to functionalization of the basal plane of 2H-MoS_2 have been established: 1) coordinative bonding to metal complexes;[32] 2) bonding of thiols and dithiols to defect sites and sulfur vacancies;[33-36] 3) reactions between diazonium radicals and vacancies; [37] and, 4) reactions with electrophilic compounds, such as maleimides, that have high selectivity towards thiols.[38]

An alternative route to MoS_2 functionalization follows conversion of 2H-MoS_2 to the metastable 1T′ phase during Li intercalation.[18-20] Li intercalation increases the nucleophilicity and reactivity of sulfur atoms on the basal plane, and enables covalent functionalization of the 1T′-MoS_2 surface using alkyl

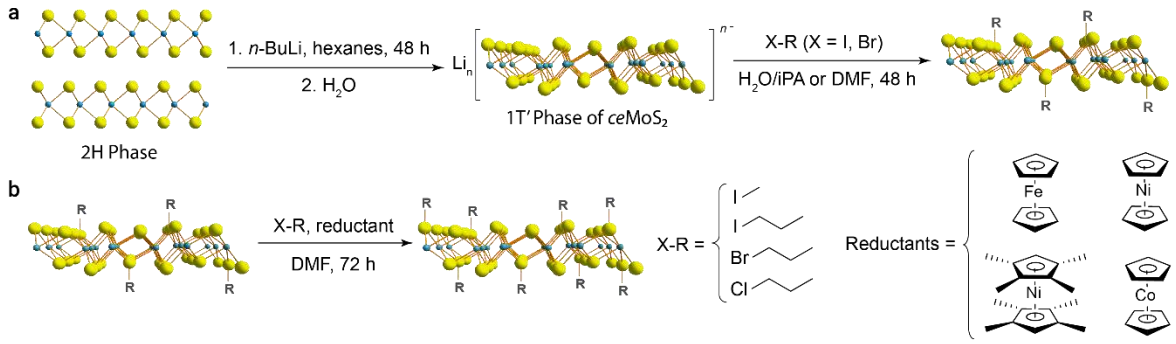

Figure 1. Synthesis of covalently functionalized 1T′-MoS_2 nanosheets. (a) Intercalation of 2H-MoS_2 with *n*-butyllithium, followed by exfoliation with water and functionalization using an alkyl halide (X-R). (b) Reductant-activated functionalization using a one-electron metallocene reductant enables further functionalization of MoS_2 nanosheets. For this report, we used the X-R molecules and reductants listed in the figure and the X-R molecule used in step (b) was the same as in (a), however functionalization using two different R groups is possible.

halide electrophiles (Figure 1a) or nucleophilic thiol reagents such as thiobarbituric acid.[18-20, 39-41] Although 2H-MoS_2 does not readily undergo these reactions, covalent functionalization of 2H-MoS_2 has been reported using iodobenzene in the presence of a palladium catalyst.[41] The coverage of functional groups achieved after chemical exfoliation is limited to <25-30% per MoS_2 unit, presumably due to the limited negative charge that can be held by the nanosheets after lithiation and exfoliation in water.[18, 21] The percent coverage is calculated from the percentage of sulfur atoms functionalized in the sample expressed per MoS_2 unit, and is not easily translated to the concept of a monolayer surface coverage, since the thickness of suspended *ce*MoS_2 flakes in solution is a distribution ranging from monolayer to few-layer. Theoretical studies of 1T-MoS_2 functionalization suggest that double-sided hydrogenation and functionalization with various functional groups can stabilize the 1T phase in favor of the 2H phase,[42] and suggest that the coverage may also modulate the band gap depending on the functional group.[43] These results provide precedent for further experimental work, noting however that the theoretical studies were performed on the perfectly octahedral (non-distorted) 1T phase rather than the distorted 1T′ phase observed experimentally after lithium intercalation with which we are primarily concerned.

Herein we describe a method of reductant-activated functionalization of *ce*MoS_2, which contains a mixture of 1T′ and 2H phases, using one-electron metallocenes, expanding on previously reported covalent functionalization procedures (Figure 1b). Detailed experimental procedures are provided in the Supplementary Information. Briefly, 2H-MoS_2 was chemically exfoliated using *n*-butyllithium to yield *ce*MoS_2, to which an excess of an alkyl halide was added, as shown in Figure 1a. For reductant-activated functionalization, one-electron metallocenes were introduced to *N*,*N*-dimethylformamide (DMF) suspensions of the functionalized MoS_2, following the initial reaction with an alkyl halide (Figure 1b). The reductant-activated functionalization increases the coverage of covalently bound functional groups on *ce*MoS_2, allows the coverage to be tuned by varying the strength of the reductant and the size of the functional group, and enables functionalization by weak electrophiles that are otherwise unreactive with 1T′-MoS_2. Use of DMF as the solvent ensured compatibility with the electrophiles and reductants used in subsequent reaction steps. Figure S2 shows that the coverage of methyl-functionalized *ce*MoS_2 (methyl-MoS_2) was the same whether water/isopropanol[18] or DMF was used as the solvent. Although palladium catalysts have been used to functionalize 2H-MoS_2 and metal chalcogenide nanoparticles with iodobenzene,[41, 44] we have observed that functionalization of 2H-MoS_2 using one-electron metallocenes does not proceed as readily as for 1T′-MoS_2. The details of how the strength of the metallocene reductant affects the functionalization of 2H-MoS_2 remains an area of active interest.

The organic moieties of functionalized MoS_2 were characterized using attenuated total reflection Fourier-transform infrared spectroscopy (ATR-FTIR) and solid-state ^{13}C cross-polarization magic-angle spinning nuclear magnetic resonance spectroscopy (^{13}C-CPMAS NMR). The coverages were quantified by fitting the multiple peaks in the sulfur 2*p* high-resolution X-ray photoelectron spectra (XPS) with the peaks at ~ 162.4 eV binding energy assigned to sulfur bound to carbon (S-C). No additional peaks were observed at higher binding energies relative to the 2H-MoS_2 sulfur peak at 163.2 eV, suggesting a lack of functionalization for the 2H phase consistent with previous studies showing that 2H-MoS_2 could not be functionalized with iodoacetamide.[18] Detailed peak-fitting parameters are provided in the Supplementary Information.

Figure 2 shows the XPS, ATR-FTIR, and ^{13}C-CPMAS NMR for *ce*MoS_2 before and after functionalization by iodomethane (methyl-MoS_2), 1-iodopropane (propyl-MoS_2), 1-bromopropane (propyl-MoS_2), and 1-chloropropane. This set of reagents was chosen to explore the dependence of reactivity on the leaving group. Consistent with previous reports of covalent functionalization of *ce*MoS_2, the proportion of 1T′ to 2H in the functionalized product remained the same after functionalization (Figure S12) and the Raman spectra for functionalized *ce*MoS_2 was similar to that of pure *ce*MoS_2 (Figure S3). No notable photoluminescence (PL) was observed before or after functionalization in the 2H or 1T′ phase at the typical PL energy range for MoS_2 mono- and few-layers (~ 600-650 nm or 1.9-2.1 eV)[26] due to the defect-rich nature of the powder 2H-MoS_2 starting material (Figure S4). In addition to the 1T′ and 2H MoS_2 phases, a shoulder was observed at a binding energy of ~ 160.8 eV in *ce*MoS_2, in accord with the binding energy of Li_2S, which can form during lithiation.[45] This peak may also be due to the formation of inner-edge defects (S*) from desulfurization during lithiation, as the generation of vacancies tends to shift the sulfur peak to lower binding energy.[46] This shoulder accounts for ~ 3% of the total sulfur in *ce*MoS_2. High-resolution spectra in the molybdenum and halide regions (Figure S5) showed no evidence of changes to the mol-

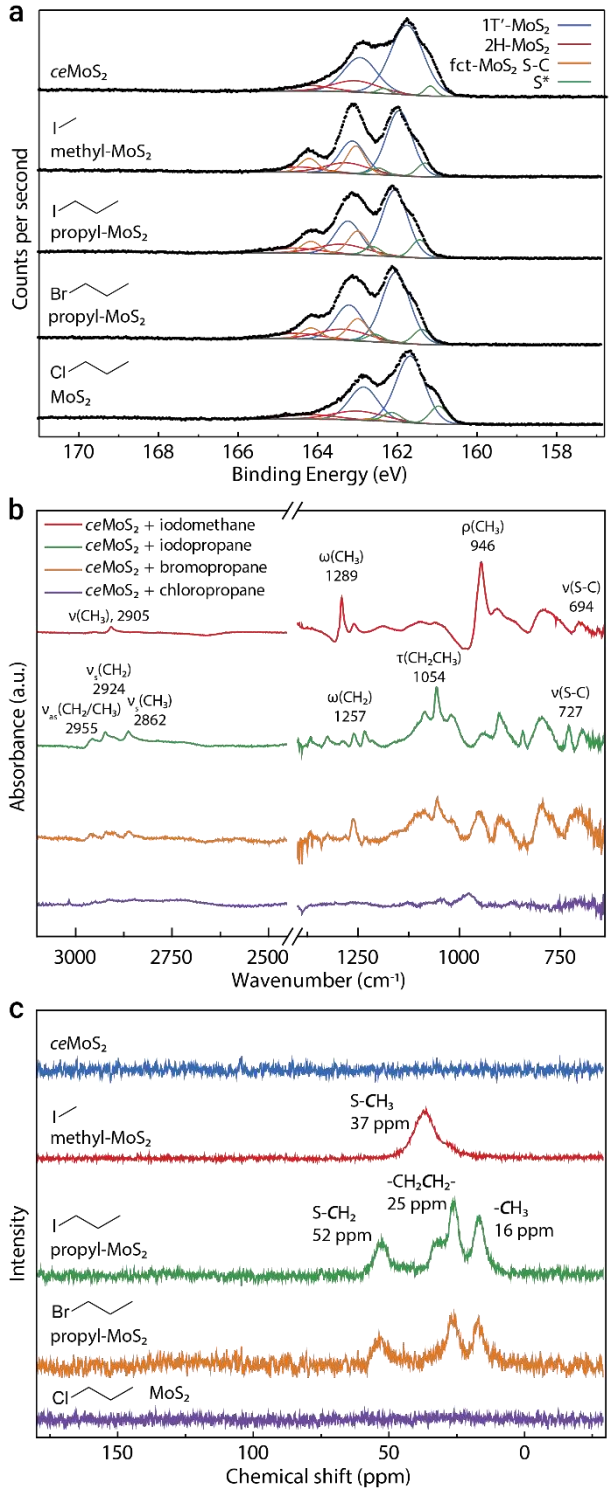

Figure 2. (a) High-resolution XPS S 2*p*, (b) ATR-FTIR, and (c) NMR spectra for *ce*MoS_2 (blue), methyl-MoS_2 from iodomethane (red), propyl-MoS_2 from iodopropane and bromopropane (green/orange), and MoS_2 after attempted reaction with chloropropane (purple). A third set sulfur peaks was present in the XPS data for functionalized MoS_2, along with characteristic C-H vibrations and carbon peaks in the ATR-FTIR and NMR spectra, respectively.

ybdenum oxidation states, and showed minimal residual halide, indicating removal of the reactant alkyl halide. The C 1*s* peak was convoluted with peaks from adventitious carbon, unlike the

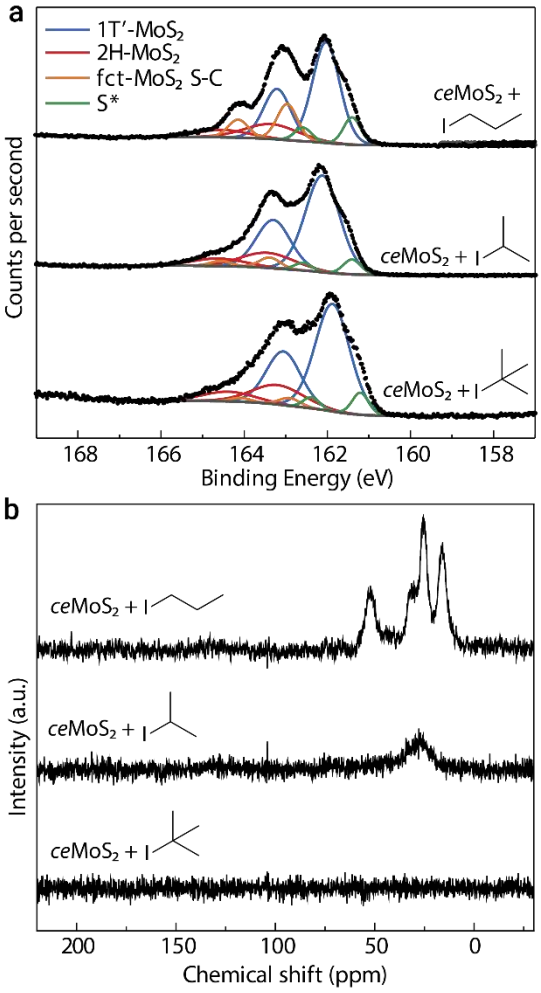

Figure 3. (a) High-resolution XPS S 2*p* spectra and (b) ^{13}C-CPMAS NMR spectra of the products from reactions between 1T′-MoS_2 and 1-iodopropane (top), 2-iodopropane (middle), and 2-iodo-2-methylpropane (bottom). Functionalization was minimal using 2-iodopropane and was unsuccessful using 2-iodo-2-methylpropane.

previously reported acetamide-MoS_2 functionalizations in which the carbonyl group was shifted to significantly higher energy and observed in the C 1*s* spectrum (Figure S6).[18]

Characteristic methyl and methylene peaks associated with methyl and propyl moieties were observed in the IR and NMR spectra (Figure 2b-c). The coverage for methyl-MoS_2 was 38% ± 0.3% (95% confidence interval, N = 3), consistent with published results for the maximum achievable coverage using iodomethane and *ce*1T′-MoS_2.[18] The characteristic IR vibrations for the C-S bond stretch, C-H bend, and C-H stretches were at 694, 946/1289, and 2905 cm^{-1} for methyl-MoS_2, and were at 727, 1257, and 2862/2924/2955 cm^{-1} for propyl-MoS_2. These peak assignments were made based on DFT calculations for optimized methanethiol and propanethiol (Table S1), to simulate the C-S bond. Furthermore, the carbon peaks at 37 ppm and 52 ppm in the NMR spectra of ^{13}C-methyl-MoS_2 (synthesized from iodomethane-^{13}C) and propyl-MoS_2, respectively, are expected for carbons covalently bound to a sulfur atom, as thiols and sulfinic acids deshield the α-carbon and cause a downfield shift in the carbon peak.[47] The two other types of carbon for propyl-MoS_2 synthesized from either io dopropane or bromopropane were also observed, at 16 ppm and

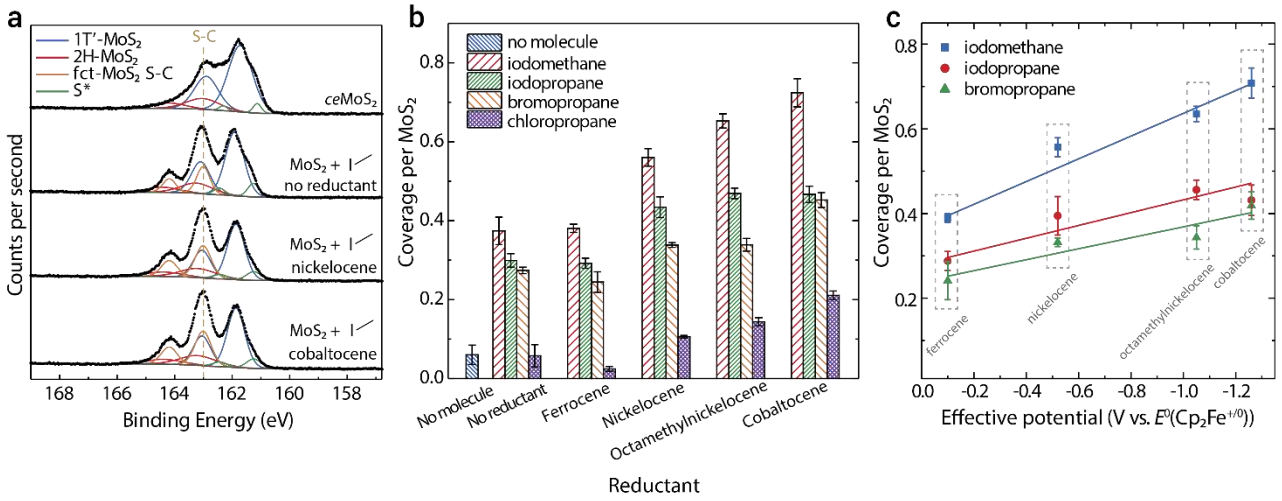

Figure 4. (a) High-resolution XPS S 2*p* spectra comparing (from top to bottom): exfoliated unfunctionalized *ce*MoS_2, methyl-MoS_2 without reductant, methyl-MoS_2 synthesized with nickelocene, and methyl-MoS_2 synthesized with cobaltocene. Peak areas from covalently functionalized sulfur were used to quantify the coverages plotted in (b) and (c). The area of the peaks for 2H-MoS_2 were constrained for all spectra to be the same percentage of total sulfur as the *ce*MoS_2 spectra. (b) Coverage per MoS_2 for MoS_2 functionalized with iodomethane, 1-iodopropane, 1-bromopropane, and 1-chloropropane for various synthetic conditions, quantified by XPS. Error bars are the standard deviations based on at least three samples. (c) Coverage per MoS_2 unit for MoS_2 functionalized with iodomethane, 1-iodopropane, 1-bromopropane as a function of the effective potential for the reductants ferrocene, nickelocene, octamethylnickelocene, and cobaltocene, corresponding to -0.10, -0.52, -1.05, and -1.26 V vs. $E^0(Fc^{+/0})$.

25 ppm, respectively. In contrast, after reaction of MoS_2 with chloropropane, the NMR spectrum indicated a lack of carbon, and no functionalized sulfur peaks or C-H vibrations were observable in the XPS and IR spectra. The reactivity of alkyl halide electrophiles with good leaving groups, such as iodine or bromine, was clearly larger than the (lack of) reactivity of alkyl halides with poor leaving groups such as chlorine. The reactivity of *ce*MoS_2 with primary, secondary, and tertiary alkyl halides was compared using 1-iodopropane, 2-iodopropane, and 2-iodo-2-methylpropane, respectively. The XP and NMR spectra for these reactions indicated that 2-iodopropane reacted minimally with *ce*MoS_2 whereas 2-iodo-2-methylpropane was unreactive (Figure 3) for the reaction shown in Figure 1a. Therefore, primary alkyl halides with an iodide or bromide leaving group are the most promising reagents for reductant-activated functionalization of 1T′-MoS_2.

The proposed origin of the driving force in the reaction of exfoliated 1T′-MoS_2 with primary alkyl iodides is negative charge that is transferred to, and stored in, the *ce*MoS_2 sheets during the lithiation step. Cation precipitation indicates that the stored negative charge ranges from 0.2-0.4 electrons per MoS_2.[21, 48] To ascertain whether the coverage achieved for methyl-MoS_2 (38% per MoS_2 or 19% per sulfur) reflected a sterically limited packing density or a limitation due to the charge density that can be stored by the sheets, *ce*MoS_2 was oxidized by stirring in DMF containing ferrocenium tetrafluoroborate for 3 days, prior to reaction of the *ce*MoS_2 with iodomethane. The overall composition of the products showed a 15% increase in 2H-MoS_2 and a 15% decrease in sulfur-carbon bonds relative to *ce*MoS_2 handled in a nominally identical way but not exposed to ferrocenium tetrafluoroborate, which showed a coverage of 35%, as expected (Figure S7). These results suggest that removal of negative charge reduces the charge available for covalent functionalization and destabilizes the 1T′ phase, favoring reversion to the 2H phase. This reasoning is consistent with the hypothesis that the 2H to 1T′ phase transformation occurs due to the stabilization of the 1T′ phase by negative charge injection.

We sought to evaluate whether an appropriately chosen reducing agent could transfer negative charge to *ce*MoS_2 or functionalized MoS_2, thereby enabling further functionalization after consumption of the initially stored negative charge. The coverage produced by functionalization was thus determined as a function of the reducing strength of the metallocenes present during the functionalization reaction.

Four metallocenes: ferrocene (Cp_2Fe), nickelocene (Cp_2Ni), octamethylnickelocene (Me_8Cp_2Ni), and cobaltocene (Cp_2Co), provided reduction potentials that spanned a range from above to below the Fermi levels ($\mathbf{E}_F$) of *ce*-, methyl-, and propyl-MoS_2, as estimated from ultraviolet photoelectron spectroscopy (UPS) (Figure S8). The effective reduction potentials, E_{eff}, of the metallocene solutions ranged from -0.1 to -1.3 V vs. ferrocenium/ferrocene ($Fc^{+/0}$), as detailed in Table S2. E_{eff} of the reactant solution was estimated by assuming a reductant: oxidant concentration ratio of 50:1 (Table S2).[49]

Figure 4 describes the change in functional group coverage as a function of the strength of the reductant. To assess the significance of the area under the fitted S-C curve, unfunctionalized *ce*MoS_2 spectra, in which the C-S bond is absent, were fit with the additional sulfur peaks at the S-C binding energy (Figure S9), generating the left-most bar in Figure 4b. All reactions were performed in triplicate with error bars indicating the standard deviation. Figure S12 shows the standard deviations of the peak areas (~ 1-3%) obtained from Monte Carlo simulations for each sample, indicating that the trends observable in Figure 4b are well outside the range of error that can be attributed to errors in XPS peak fitting. In addition to quantification by XPS, ^{13}C MAS NMR on *ce*MoS_2 functionalized with ^{13}C-iodomethane with and without

nickelocene and cobaltocene, verified the trend of increasing coverage with reductant strength (Figure S10).

The effective potential of the ferrocene solution was slightly below the estimated Fermi level of *ce*MoS_2 (Figure S8, Table S2). As expected, exposure to the ferrocene solution did not result in a substantial change in coverage. Figure 4c shows an approximately linear increase in coverage for iodomethane, iodopropane, and bromopropane as the strength of the reductant was increased from ferrocene (E_{eff} = -0.12 V vs. $Fc^{+/0}$) to cobaltocene (E_{eff} = -1.3 V vs. $Fc^{+/0}$). For reactions involving chloropropane, S-C bonds were only visible in the XPS data after reactions performed in the presence of cobaltocene, the strongest reductant examined. Due to the similarity of some XP spectra to spectra for unfunctionalized *ce*MoS_2, ^{13}C NMR and ATR-FTIR were used to verify that functionalization was successful using cobaltocene, whereas minimal coverage resulted when octamethylnickelocene was used (Figure S11). Notably, the NMR peak positions and peak splitting for propyl-MoS_2 synthesized using chloropropane and cobaltocene were in accord with those for propyl-MoS_2 shown in Figure 2; however, an additional peak was present at 87 ppm, and the intensity of the peak at 54 ppm was relatively small, consistent with a downfield shift for the anchoring carbon which can be observed in R-CH_2-O species. An additional 4% of both molybdenum and sulfur oxides were observed in the XPS data for the chloropropane/cobaltocene functionalization compared to functionalization using iodopropane, further suggesting a linkage through metal or sulfur oxides. The fraction of MoS_2 in the 1T′ phase was ~ 90% for all conditions (Figure S12).

To investigate whether higher coverages could be obtained, decamethylcobaltocene ($Me_{10}Cp_2Co$), E_{eff} = -1.9 V vs. $Fc^{+/0}$, was also used for the synthesis of methyl-MoS_2. However, the coverage did not increase substantially compared to when cobaltocene was used (Figure S12), and the highest achievable coverage was thus 70%. DFT modeling of the packing and further experiments will be helpful in understanding the upper coverage limit produced by this reaction pathway.

Understanding how to control coverage and achieve high densities is important for using functionalized surfaces to control corrosion or recombination at edge sites; to create surface dipoles to tune relative band positions; to introduce chemically reactive handles for subsequent functionalization; and for use of such surfaces as absorption sensors. Any application that relies on the effects or signals produced by the functionalized surface requires quantitative control of the surface coverage. In addition to understanding the charge transfer and fundamental surface chemistry of *ce*MoS_2 by using one-electron reductants, the reductant-activated functionalization method reported herein introduces additional control for mixed-functionalization surfaces. The method may be extended beyond MoS_2, and the use of different functional groups in the two steps allows for development of multi-functional surfaces.

In summary, we have shown that primary alkyl halides with an iodide or bromide leaving groups are the most promising reagents for reductant-activated functionalization of 1T′-MoS_2, and that either removal or addition of negative charge on the *ce*MoS_2 will decrease or increase the amount of functionalization achieved. Further, a reductant-activated functionalization method has been developed that allows for control over the degree of coverage of covalently attached surface functional groups on 1T′-MoS_2 and enables functionalization by weak electrophiles that are otherwise non-reactive toward *ce*MoS_2. By varying the reductant strength, the coverage can be increased beyond the previous limit imposed by the amount of negative charge stored during exfoliation. Our observations that redox chemistry influences the coverage achievable during functionalization impact the understanding of the charge-transfer mechanisms governing surface functionalization and will inform and stimulate further mechanistic studies. Future studies of the applicability of this method to the covalent functionalization of similar layered materials and the impact of functionalization on stability would inform the application of these materials in various areas such as sensing, nanofiltration, and drug delivery.

ASSOCIATED CONTENT

Supporting Information. The Supporting Information is available free of charge on the ACS Publications website at http://pubs.acs.org.

Experimental details; supporting Figures S1-S13 and Tables S1-S2 (PDF).

AUTHOR INFORMATION

Corresponding Author

* E-mail: nslewis@caltech.edu. Tel: (626) 395-6335.

Notes

The authors declare no competing financial interests.

ACKNOWLEDGMENT

This work was supported by the U.S. Department of Energy, Office of Basic Energy Sciences under award no. DE-FG02-03ER15483. E.X.Y. gratefully acknowledges Dr. Sonjong Hwang at the Caltech Solid-State NMR Facility for discussions and NMR spectra. Research was in part carried out at the Molecular Materials Research Center of the Beckman Institute of the California Institute of Technology. Computations were performed with assistance from the Goddard group at Caltech.

REFERENCES

(1) Nicolosi, V.; Chhowalla, M.; Kanatzidis, M. G.; Strano, M. S.; Coleman, J. N. Liquid Exfoliation of Layered Materials. *Science* **2013,** *340*, 1226419.

(2) Kim, Y.; Bark, H.; Ryu, G. H.; Lee, Z.; Lee, C. Wafer-scale monolayer MoS_2 grown by chemical vapor deposition using a reaction of MoO_3 and H_2S. *J. Phys. Condens. Matter* **2016,** *28*, 184002.

(3) Duan, X.; Wang, C.; Pan, A.; Yu, R.; Duan, X. Two-dimensional transition metal dichalcogenides as atomically thin semiconductors: opportunities and challenges. *Chem. Soc. Rev.* **2015,** *44*, 8859-8876.

(4) Li, M. Y.; Shi, Y. M.; Cheng, C. C.; Lu, L. S.; Lin, Y. C.; Tang, H. L.; Tsai, M. L.; Chu, C. W.; Wei, K. H.; He, J. H.; Chang, W. H.; Suenaga, K.; Li, L. J. Epitaxial growth of a monolayer WSe_2-MoS_2 lateral p-n junction with an atomically sharp interface. *Science* **2015,** *349*, 524-528.

(5) Gong, C.; Zhang, H.; Wang, W.; Colombo, L.; Wallace, R. M.; Cho, K. Band alignment of two-dimensional transition metal dichalcogenides: Application in tunnel field effect transistors. *Appl. Phys. Lett.* **2013,** *103*, 053513.

(6) Heine, T. Transition metal chalcogenides: ultrathin inorganic materials with tunable electronic properties. *Acc. Chem. Res.* **2015,** *48*, 65-72.

(7) Wu, S.; Zeng, Z.; He, Q.; Wang, Z.; Wang, S. J.; Du, Y.; Yin, Z.; Sun, X.; Chen, W.; Zhang, H. Electrochemically reduced single-layer MoS_2 nanosheets: characterization, properties, and sensing applications. *Small* **2012,** *8*, 2264-2270.

(8) Samnakay, R.; Jiang, C.; Rumyantsev, S. L.; Shur, M. S.; Balandin, A. A. Selective chemical vapor sensing with few-layer MoS_2

thin-film transistors: Comparison with graphene devices. *Appl. Phys. Lett.* **2015,** *106*, 023115.

(9) Li, H.; Yin, Z.; He, Q.; Li, H.; Huang, X.; Lu, G.; Fam, D. W. H.; Tok, A. I. Y.; Zhang, Q.; Zhang, H. Fabrication of Single- and Multilayer MoS_2 Film-Based Field-Effect Transistors for Sensing NO at Room Temperature. *Small* **2012,** *8*, 63-67.

(10) Ries, L.; Petit, E.; Michel, T.; Diogo, C. C.; Gervais, C.; Salameh, C.; Bechelany, M.; Balme, S.; Miele, P.; Onofrio, N.; Voiry, D. Enhanced sieving from exfoliated MoS2 membranes via covalent functionalization. *Nat. Mater.* **2019,** *18*, 1112-1117.

(11) Chen, Y.; Tan, C.; Zhang, H.; Wang, L. Two-dimensional graphene analogues for biomedical applications. *Chem. Soc. Rev.* **2015,** *44*, 2681-2701.

(12) Yadav, V.; Roy, S.; Singh, P.; Khan, Z.; Jaiswal, A. 2D MoS_2-Based Nanomaterials for Therapeutic, Bioimaging, and Biosensing Applications. *Small* **2019,** *15*, 1803706.

(13) Britto, R. J.; Benck, J. D.; Young, J. L.; Hahn, C.; Deutsch, T. G.; Jaramillo, T. F. Molybdenum Disulfide as a Protection Layer and Catalyst for Gallium Indium Phosphide Solar Water Splitting Photocathodes. *J. Phys. Chem. Lett.* **2016,** *7*, 2044-2049.

(14) Kwon, K. C.; Choi, S.; Hong, K.; Moon, C. W.; Shim, Y.-S.; Kim, D. H.; Kim, T.; Sohn, W.; Jeon, J.-M.; Lee, C.-H.; Nam, K. T.; Han, S.; Kim, S. Y.; Jang, H. W. Wafer-scale transferable molybdenum disulfide thin-film catalysts for photoelectrochemical hydrogen production. *Energy Environ. Sci.* **2016,** *9*, 2240-2248.

(15) Voiry, D.; Salehi, M.; Silva, R.; Fujita, T.; Chen, M.; Asefa, T.; Shenoy, V. B.; Eda, G.; Chhowalla, M. Conducting MoS_2 Nanosheets as Catalysts for Hydrogen Evolution Reaction. *Nano Lett.* **2013,** *13*, 6222-6227.

(16) Kalantar-zadeh, K.; Ou, J. Z.; Daeneke, T.; Strano, M. S.; Pumera, M.; Gras, S. L. Two-Dimensional Transition Metal Dichalcogenides in Biosystems. *Adv. Funct. Mater.* **2015,** *25*, 5086-5099.

(17) Toh, R. J.; Sofer, Z.; Luxa, J.; Sedmidubský, D.; Pumera, M. 3R phase of MoS_2 and WS_2 outperforms the corresponding 2H phase for hydrogen evolution. *Chem. Commun.* **2017,** *53*, 3054-3057.

(18) Voiry, D.; Goswami, A.; Kappera, R.; Silva, C. d. C. C. e.; Kaplan, D.; Fujita, T.; Chen, M.; Asefa, T.; Chhowalla, M. Covalent functionalization of monolayered transition metal dichalcogenides by phase engineering. *Nat. Chem.* **2015,** *7*, 45-49.

(19) Knirsch, K. C.; Berner, N. C.; Nerl, H. C.; Cucinotta, C. S.; Gholamvand, Z.; McEvoy, N.; Wang, Z.; Abramovic, I.; Vecera, P.; Halik, M.; Sanvito, S.; Duesberg, G. S.; Nicolosi, V.; Hauke, F.; Hirsch, A.; Coleman, J. N.; Backes, C. Basal-Plane Functionalization of Chemically Exfoliated Molybdenum Disulfide by Diazonium Salts. *ACS Nano* **2015,** *9*, 6018-6030.

(20) Benson, E. E.; Zhang, H.; Schuman, S. A.; Nanayakkara, S. U.; Bronstein, N. D.; Ferrere, S.; Blackburn, J. L.; Miller, E. M. Balancing the Hydrogen Evolution Reaction, Surface Energetics, and Stability of Metallic MoS_2 Nanosheets via Covalent Functionalization. *J. Am. Chem. Soc.* **2018,** *140*, 441-450.

(21) Heising, J.; Kanatzidis, M. G. Exfoliated and Restacked MoS_2 and WS_2: Ionic or Neutral Species? Encapsulation and Ordering of Hard Electropositive Cations. *J. Am. Chem. Soc.* **1999,** *121*, 11720-11732.

(22) Qin, X. R.; Yang, D.; Frindt, R. F.; Irwin, J. C. Real-space imaging of single-layer MoS_2 by scanning tunneling microscopy. *Phys. Rev. B* **1991,** *44*, 3490-3493.

(23) Chou, S. S.; Sai, N.; Lu, P.; Coker, E. N.; Liu, S.; Artyushkova, K.; Luk, T. S.; Kaehr, B.; Brinker, C. J. Understanding catalysis in a multiphasic two-dimensional transition metal dichalcogenide. *Nat. Commun.* **2015,** *6*, 8311.

(24) Calandra, M. Chemically exfoliated single-layer MoS_2: Stability, lattice dynamics, and catalytic adsorption from first principles. *Phys. Rev. B* **2013,** *88*, 245428.

(25) Fan, X.-L.; Yang, Y.; Xiao, P.; Lau, W.-M. Site-specific catalytic activity in exfoliated MoS_2 single-layer polytypes for hydrogen evolution: basal plane and edges. *J. Mater. Chem. A* **2014,** *2*, 20545-20551.

(26) Eda, G.; Yamaguchi, H.; Voiry, D.; Fujita, T.; Chen, M.; Chhowalla, M. Photoluminescence from chemically exfoliated MoS_2. *Nano Lett.* **2011,** *11*, 5111-5116.

(27) Fan, X. B.; Xu, P. T.; Zhou, D. K.; Sun, Y. F.; Li, Y. G. C.; Nguyen, M. A. T.; Terrones, M.; Mallouk, T. E. Fast and Efficient Preparation of Exfoliated 2H MoS_2 Nanosheets by Sonication-Assisted Lithium Intercalation and Infrared Laser-Induced 1T to 2H Phase Reversion. *Nano Lett.* **2015,** *15*, 5956-5960.

(28) Royea, W. J.; Juang, A.; Lewis, N. S. Preparation of air-stable, low recombination velocity Si(111) surfaces through alkyl termination. *Appl. Phys. Lett.* **2000,** *77*, 1988-1990.

(29) Plymale, N. T.; Ramachandran, A. A.; Lim, A.; Brunschwig, B. S.; Lewis, N. S. Control of the Band-Edge Positions of Crystalline Si(111) by Surface Functionalization with 3,4,5-Trifluorophenylacetylenyl Moieties. *J. Phys. Chem. C* **2016,** *120*, 14157-14169.

(30) Gleason-Rohrer, D. C.; Brunschwig, B. S.; Lewis, N. S. Measurement of the band bending and surface dipole at chemically functionalized Si(111)/vacuum interfaces. *J. Phys. Chem. C* **2013,** *117*, 18031-18042.

(31) O'Leary, L. E.; Strandwitz, N. C.; Roske, C. W.; Pyo, S.; Brunschwig, B. S.; Lewis, N. S. Use of Mixed CH_3-/$HC(O)CH_2CH_2$-Si(111) Functionality to Control Interfacial Chemical and Electronic Properties During the Atomic-Layer Deposition of Ultrathin Oxides on Si(111). *J. Phys. Chem. Lett.* **2015,** *6*, 722-726.

(32) Backes, C.; Berner, N. C.; Chen, X.; Lafargue, P.; LaPlace, P.; Freeley, M.; Duesberg, G. S.; Coleman, J. N.; McDonald, A. R. Functionalization of Liquid-Exfoliated Two-Dimensional 2H-MoS_2. *Angew. Chem. Int. Ed.* **2015,** *54*, 2638-2642.

(33) Chou, S. S.; De, M.; Kim, J.; Byun, S.; Dykstra, C.; Yu, J.; Huang, J.; Dravid, V. P. Ligand Conjugation of Chemically Exfoliated MoS_2. *J. Am. Chem. Soc.* **2013,** *135*, 4584-4587.

(34) Nguyen, E. P.; Carey, B. J.; Ou, J. Z.; van Embden, J.; Gaspera, E. D.; Chrimes, A. F.; Spencer, M. J. S.; Zhuiykov, S.; Kalantar-zadeh, K.; Daeneke, T. Electronic Tuning of 2D MoS_2 through Surface Functionalization. *Adv. Mater.* **2015,** *27*, 6225-6229.

(35) Chen, X.; Berner, N. C.; Backes, C.; Duesberg, G. S.; McDonald, A. R. Functionalization of Two-Dimensional MoS_2: On the Reaction Between MoS_2 and Organic Thiols. *Angew. Chem. Int. Ed.* **2016,** *55*, 5803-5808.

(36) Ding, Q.; Czech, K. J.; Zhao, Y.; Zhai, J.; Hamers, R. J.; Wright, J. C.; Jin, S. Basal-Plane Ligand Functionalization on Semiconducting 2H-MoS_2 Monolayers. *ACS Appl. Mater. Interfaces* **2017,** *9*, 12734-12742.

(37) Chu, X. S.; Yousaf, A.; Li, D. O.; Tang, A. A.; Debnath, A.; Ma, D.; Green, A. A.; Santos, E. J. G.; Wang, Q. H. Direct Covalent Chemical Functionalization of Unmodified Two-Dimensional Molybdenum Disulfide. *Chem. Mater.* **2018,** *30*, 2112-2128.

(38) Vera-Hidalgo, M.; Giovanelli, E.; Navío, C.; Pérez, E. M. Mild Covalent Functionalization of Transition Metal Dichalcogenides with Maleimides: A "Click" Reaction for 2H-MoS_2 and WS_2. *J. Am. Chem. Soc.* **2019**, *141,* 3767-3771.

(39) Tuci, G.; Mosconi, D.; Rossin, A.; Luconi, L.; Agnoli, S.; Righetto, M.; Pham-Huu, C.; Ba, H.; Cicchi, S.; Granozzi, G.; Giambastiani, G. Surface Engineering of Chemically Exfoliated MoS_2 in a "Click": How To Generate Versatile Multifunctional Transition Metal Dichalcogenides-Based Platforms. *Chem. Mater.* **2018,** *30*, 8257-8269.

(40) Presolski, S.; Wang, L.; Loo, A. H.; Ambrosi, A.; Lazar, P.; Ranc, V.; Otyepka, M.; Zboril, R.; Tomanec, O.; Ugolotti, J.; Sofer, Z.; Pumera, M. Functional Nanosheet Synthons by Covalent Modification of Transition-Metal Dichalcogenides. *Chem. Mater.* **2017,** *29*, 2066-2073.

(41) Vishnoi, P.; Sampath, A.; Waghmare, U. V.; Rao, C. N. R. Covalent Functionalization of Nanosheets of MoS_2 and $MoSe_2$ by Substituted Benzenes and Other Organic Molecules. *Chem.: Eur. J.* **2017,** *23*, 886-895.

(42) Qu, Y.; Pan, H.; Kwok, C. T. Hydrogenation-controlled phase transition on two-dimensional transition metal dichalcogenides and their unique physical and catalytic properties. *Sci. Rep.* **2016,** *6*, 34186.

(43) Tang, Q.; Jiang, D.-e. Stabilization and Band-Gap Tuning of the 1T-MoS_2 Monolayer by Covalent Functionalization. *Chem. Mater.* **2015,** *27*, 3743-3748.

(44) Vishnoi, P.; Fatahi, P.; Barua, M.; Bandyopadhyay, A.; Pati, S. K.; Rao, C. N. R. Covalently Functionalized Nanoparticles of Semiconducting Metal Chalcogenides and Their Attributes. *ChemNanoMat* **2018,** *4*, 41-45.

(45) Fantauzzi, M.; Elsener, B.; Atzei, D.; Rigoldi, A.; Rossi, A. Exploiting XPS for the identification of sulfides and polysulfides. *RSC Adv.* **2015,** *5*, 75953-75963.

(46) Li, H.; Tsai, C.; Koh, A. L.; Cai, L.; Contryman, A. W.; Fragapane, A. H.; Zhao, J.; Han, H. S.; Manoharan, H. C.; Abild-Pedersen, F.; Nørskov, J. K.; Zheng, X. Activating and optimizing MoS2 basal planes for hydrogen evolution through the formation of strained sulphur vacancies. *Nat. Mater.* **2015,** *15*, 48-53.

(47) Freeman, F.; Angeletakis, C. N. ^{13}C NMR chemical shifts of thiols, sulfinic acids, sulfinyl chlorides, sulfonic acids and sulfonic anhydrides. *Org. Magn. Reson.* **1983,** *21*, 86-93.

(48) Gash, A. E.; Spain, A. L.; Dysleski, L. M.; Flaschenriem, C. J.; Kalaveshi, A.; Dorhout, P. K.; Strauss, S. H. Efficient Recovery of Elemental Mercury from Hg(II)-Contaminated Aqueous Media Using a Redox-Recyclable Ion-Exchange Material. *Environ. Sci. Technol.* **1998,** *32*, 1007-1012.

(49) Grimm, R. L.; Bierman, M. J.; O'Leary, L. E.; Strandwitz, N. C.; Brunschwig, B. S.; Lewis, N. S. Comparison of the Photoelectrochemical Behavior of H-Terminated and Methyl-Terminated Si(111) Surfaces in Contact with a Series of One-Electron, Outer-Sphere Redox Couples in CH_3CN. *J. Phys. Chem. C* **2012,** *116*, 23569-23576.

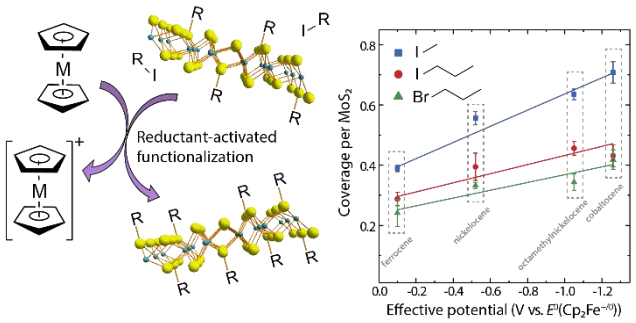
M
M
+
R
I
Reductant-activated
functionalization
I
I
Br
Coverage per MoS_2
0.8
0.6
0.4
0.2
ferrocene
nickelocene
octamethylnickelocene
cobaltocene
0.0
-0.2
-0.4
-0.6
-0.8
-1.0
-1.2
Effective potential (V vs. $E^0(Cp_2Fe^{+/0})$)